Atmospheric Environment 289 (2022) 119320

Contents lists available at ScienceDirect

Atmospheric Environment

journal homepage: www.elsevier.com/locate/atmosenv

Atmospheric fine particulate dicarboxylic acids and related SOA in winter at the background site of Yangtze River Delta: Implication for the long-distance transport of solid fuels burning

Wei Du [a,1], Zhijian Ding [a,1], Yali Lei [a], Si Zhang [a], Can Wu [a], Fan Zhang [a], Fanglin Wang [a], Shaojun Lv [a], Xiaodi Liu [a], Jingjing Meng [b], Gehui Wang [a,c,*]

[a] Key Laboratory of Geographic Information Science of the Ministry of Education, School of Geographic Sciences, East China Normal University, Shanghai, 200241, China
[b] School of Environment and Planning, Liaocheng University, Liaocheng, 252000, China
[c] Institute of Eco-Chongming, 20 Cuiniao Rd., Chenjia Zhen, Chongming, Shanghai, 202162, China

HIGHLIGHTS

- Winter dicarboxylic acids and related compounds at background Yangtze River Delta were measured.
- Aqueous phase oxidation dominated the formation of dicarboxylic acids in winter.
- Long distance transport of coal and biomass burning were the dominant sources in haze days.
- Mono-modal size distribution in winter, while bimodal size distribution of dicarboxylic acids in summer were found.

GRAPHICAL ABSTRACT

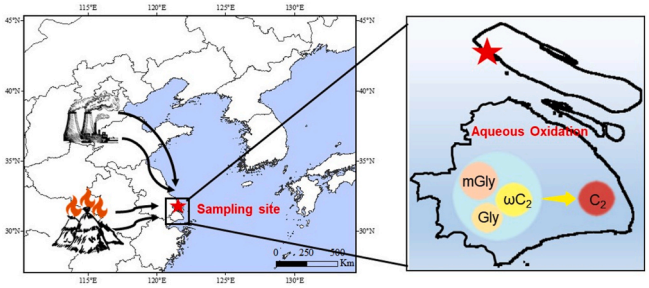

ARTICLE INFO

Keywords:
Dicarboxylic acids
Long-distance transport
Aqueous-phase oxidation
Yangtze river delta
Solid fuels

ABSTRACT

To identify the pollution characteristics of dicarboxylic acids in the background of the Yangtze River Delta (YRD) during winter, diurnal $PM_{2.5}$ samples were collected in Chongming Island, a background site of YRD nearby Shanghai and determined for organic compounds including dicarboxylic acids, organic carbon (OC), elemental carbon (EC), water-soluble organic carbon (WSOC), levoglucosan, and related inorganic ions. The total concentration of dicarboxylic acid organics was 433 ± 70 ng/m^3, of which oxalic acid was the most abundant species, followed by phthalic acid (Ph), succinic acid (C_4), and malonic acid (C_3). Four typical pollution events occurred during the campaign (defined as Event 1, Event 2, Event 3, and Event 4) were identified. The organic matters in Event 1 and Event 2 mainly came from the transport of coal burning emissions derived from northern China with space heating such as Inner Mongolia and Shandong, while those in Event 3 and Event 4 periods came from the long distance transport of biomass burning in Anhui and Henan provinces. We found that aqueous phase oxidation, instead of gaseous phase oxidation, dominated the formation of dicarboxylic acids in the region. The dicarboxylic acids followed a mono-modal size distribution pattern in winter, obviously different from that in

* Corresponding author. Key Laboratory of Geographic Information Science of the Ministry of Education, School of Geographic Sciences, East China Normal University, Shanghai, 200241, China.
E-mail address: ghwang@geo.ecnu.edu.cn (G. Wang).
[1] These authors contribute equally to this work.

https://doi.org/10.1016/j.atmosenv.2022.119320
Received 27 June 2022; Received in revised form 1 August 2022; Accepted 2 August 2022
Available online 11 August 2022

summer, mainly due to the dominant aerosol aqueous phase formation and the weak volatilization in winter with low ambient temperature. The result obtained by this study was expected to provide novel insight of source, pollution characteristics, and formation mechanism of secondary organic aerosols (SOA) in the background of YRD and benefit the pollutants control policy formulation.

1. Introduction

Dicarboxylic acids are the most thoroughly oxidized substances of ambient SOA and commonly used as tracers to indicate the aging degree of atmospheric aerosols due to high O/C ratio (Ervens et al., 2011; Wang et al., 2012). Dicarboxylic acids in the atmosphere mainly come from the secondary photochemical reactions and primary sources such as biomass and fossil fuel burning (Rogge et al., 1991; Kawamura et al., 2013). Dicarboxylic acids are abundant and ubiquitous in atmosphere aerosols due to the low vapor pressures and high hygroscopicity (Bilde et al., 2015; Kawamura and Bikkina, 2016). As water-soluble organic compounds, dicarboxylic acids are usually combined with fine particle and can act as cloud condensation nucleus (CCN) and ice nucleus (IN), thus directly affecting the global climate change (Meng et al., 2018; Zhang et al., 2016).

Dicarboxylic acid could explain the specific pollution formation process as the final product of atmospheric photochemical reaction. However, previous studies were mostly conducted in cities or mountains located in northern China (Meng et al., 2014, 2018; Yu et al., 2021). To our best knowledge, limited studies focused on the dicarboxylic acid pollution in southern China. Liu et al. (2021) investigated the vertical distribution of organic acids in Guangzhou city and found they were mainly from secondary processes and biomass burning. YRD, as a region densely populated and urbanized with a high scale of industrialization, is suffering from severe air pollution in recent years (Petaja et al., 2016; Song et al., 2017), especially in winter with unfavorable diffusion conditions. The air pollution in YRD is catching wide concern recently. For example, it was found biomass burning in winter had an important influence on haze formation in the YRD region (Haque et al., 2020). Another study in Ningbo city showed the coal combustion had a great contribution to $PM_{2.5}$ particles during the high pollution episode in wintertime (Xu et al., 2016). Unfortunately, researches on atmospheric organic aerosols mainly focused on primary pollutants such as PAHs (Cai et al., 2017; Wang et al., 2017), relatively inadequate studies focused on SOA, especially for dicarboxylic acids (Ding et al., 2021). Our previous study investigated the dicarboxylic acids in a background site of YRD in summer time, suggesting the local biomass burning and long-distance transport of VOCs were the dominant sources during the pollution period (Ding et al., 2021). It's well known that the atmospheric photochemical oxidation capacity is weaker in winter time, thus the pollution characteristics would be much different from that in summer. Considering the seasonal difference was not clear for the pollution characteristics of dicarboxylic acid, it was necessary to fill the data gap.

In this study, $PM_{2.5}$ samples were collected in Chongming Island, the world's largest estuarine alluvial island in YRD region in winter. As the sampling site is with less urbanization scale, population, and vehicles, it was regarded as an ideal atmospheric background site of YRD region. The main objective of this study is to explore the pollution characteristics of dicarboxylic acid including molecular composition, formation mechanism, and sources during winter time at a background site in YRD region, the seasonal difference was also discussed based on the comparison with our previous work (Ding et al., 2021). We hope the result of our work could provide a further insight of the dicarboxylic acids pollution and be helpful for both researchers and policy makers.

2. Experimental section

2.1. Study site and sample collection

$PM_{2.5}$ filter samples were collected from December 27, 2018 to January 25, 2019 based on a semidiurnal duration. A total of 61 $PM_{2.5}$ filter samples including 2 blank corrected filters were collected using a high-volume air sampler with a flow rate of 1.13 m^3/min (TE-6070VBLX, Tisch Environ. Inc, Cleves, OH, USA). The sampling site is located in the west beach of Chongming Island (31.7 °N, 121.2 °E), as shown in Fig. 1. There were no obvious local pollution sources near this site, which could reflect the atmospheric quality in the background area of YRD. The samples were collected every 12 h at 8:00 and 20:00 each day. The size-segregated samples were collected using a nine-stage Anderson impactor sampler with a flow rate of 28 L/min (Series 20–800, Thermo Electron Corporation, Waltham, MA, USA). The sampling duration of each set of the size-segregated samples was 72 h. The cutoff points of the size-resolved samplers were 0.43, 0.67, 1.1, 2.1, 3.3, 4.7, 5.8 and 9.0 μm, respectively (Wang et al., 2018). The collected filters were wrapped and sealed with clean aluminum foil and frozen at −20 °C prior to analysis. Before sampling, all the filters and aluminum foil were pre-baked at 450 °C for 6 h in muffle furnace to remove organic pollutants.

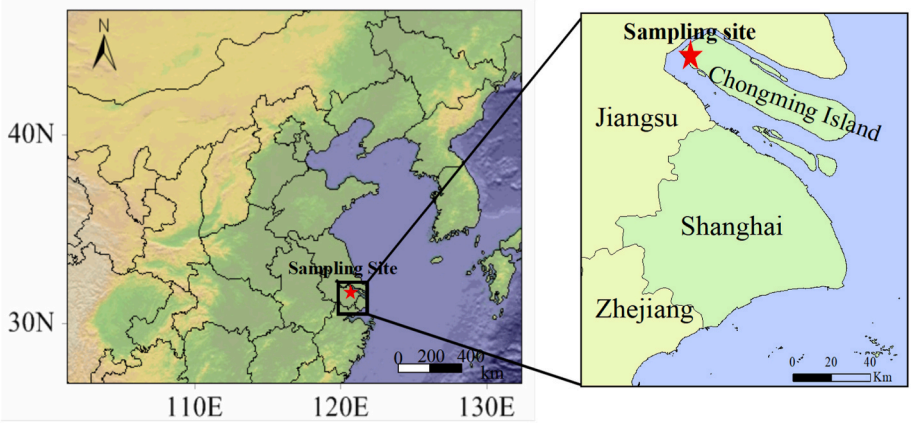

Fig. 1. Geographical location of sampling site.

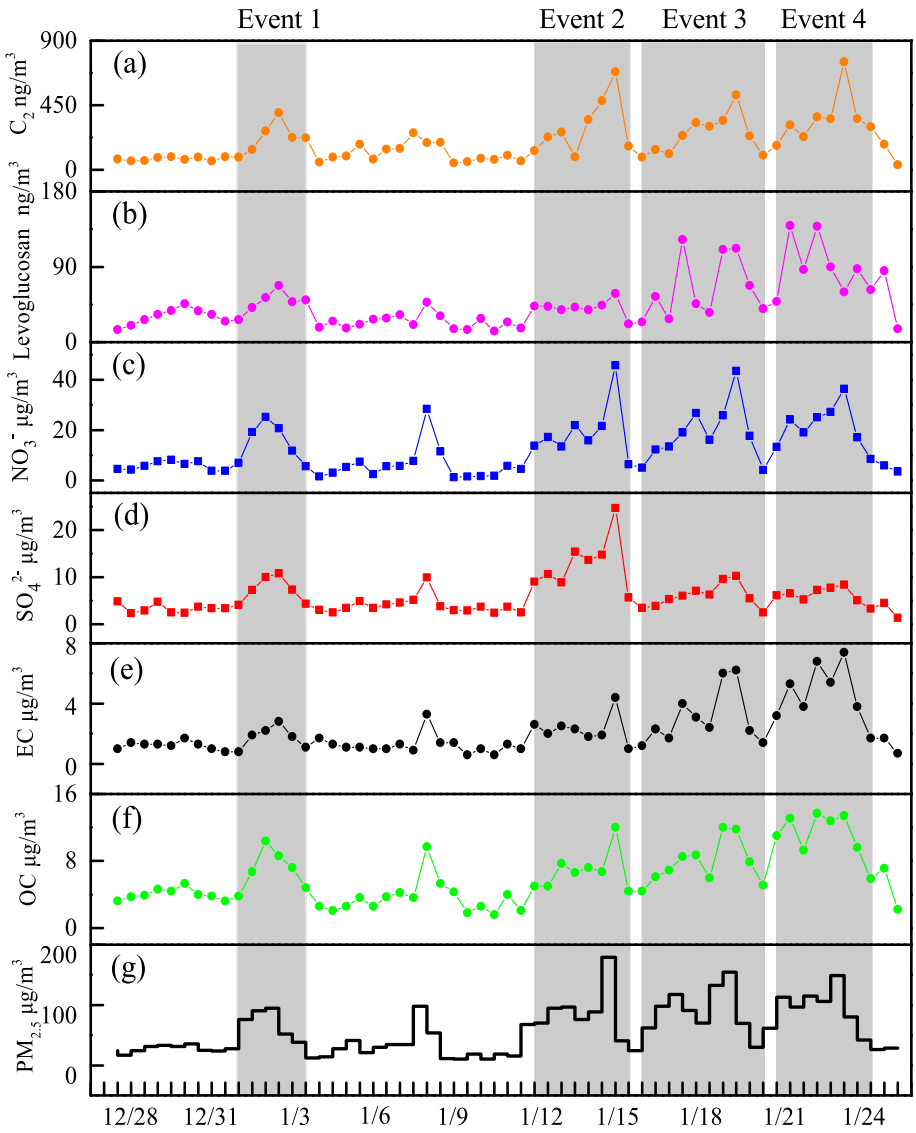

Fig. 2. Time series of the concentrations of $PM_{2.5}$ and related chemical components during sampling period in Chongming Island (The gray shadows named Event 1, 2, 3, 4 represent four different pollution events).

2.2. Sample analysis and quality control

2.2.1. Dicarboxylic acids, ketocarboxylic acids, and α-dicarbonyls

The analysis method was described in detail in our previous studies (Wang et al., 2010; Meng et al., 2013; Ding et al., 2021). According to the mass concentration of $PM_{2.5}$ in each sample, a certain area of the filter was cut into pieces and 5 mL Milli-Q water was added under ultrasonication three times each for 10 min. Then, the filtrate was evaporated until dry under 55 °C vacuum conditions. Then reacted with 14% BF_3/n-butanol solution at 100 °C for 1 h. After cooling, the derivatives were dissolved in n-hexane and washed three times with Milli-Q water, and finally the hexane solution was concentrated to 100 μL, the gas chromatographic GC (Agilent, 6890-FID) combined with FID detector was used for the quantitative analysis of the molecular composition and concentration. The GC heating procedure was as following: holding 2 min from the starting temperature of 50 °C, then increasing to 120 °C at a rate of 30 °C/min, then maintaining 10 min after increasing to 300 °C at a rate of 6 °C/min. GC/MS (Agilent, GC7890A-MS5975C) was used to identify the detected compounds. The recoveries of the dicarboxylic acids were 85% for oxalic acid and 85%–110% for other species. All the data presented in this paper were corrected for both field blanks and recoveries.

2.2.2. Elemental carbon (EC), organic carbon (OC), water-soluble organic carbon (WSOC), inorganic ions (IC) and levoglucosan

The analysis of OC and EC followed the Interagency Monitoring of Protected Visual Environments (IMPROVE) agreement of America, using DRI model 2001A carbon analyzer and TOR protocol for optical correction, and the detailed analysis method could be found elsewhere (Chow et al., 2004; Li et al., 2012). The analysis methods of WSOC and IC were as follows: a certain area of the $PM_{2.5}$ filter was cut out and placed in a centrifuge tube with 25 mL Milli-Q water. The tubes were under ultrasonication for 1 h and then on the shaking-table for 1 h, then the filtrate was extracted with a disposable syringe and filtered with a 0.45 μm filter element. WSOC was analyzed by a Total Organic Carbon analyzer (Shimadzu TOC-L CPH), and the inorganic ions were analyzed by Dionex-600 and Dionex-500 Ion Chromatographs. The analysis method of levoglucosan was derived from BSTFA and GC/MS (Agilent 5890/7593, USA) was used to quantitative analysis (Wang et al., 2011).

SPSS 21.0 (IBM Corporation, Armonk, NY, USA) was used for statistical analysis with a significance level of 0.05.

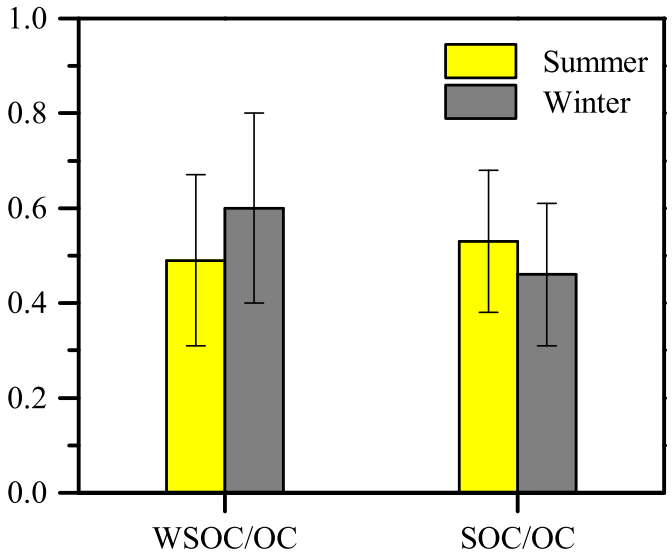

Fig. 3. Comparison of WSOC/OC and SOC/OC during the sampling period in winter and summer at Chongming Island.

3. Results and discussion

3.1. OC, EC, WSOC, SOC, IC, and $PM_{2.5}$

Fig. 2 shows the time series of the organic components concentrations and two inorganic ions in $PM_{2.5}$ samples during the whole sampling period. The average $PM_{2.5}$ concentration was 59 ± 41 μg/m^3 (ranging from 10 to 179 μg/m^3). According to the national ambient air quality standard of China (GB 3095–2012), 56% of the samples exceeded the first limit concentration (35 μg/m^3), indicating relatively serious $PM_{2.5}$ pollution during the campaign. It is recognized that EC is derived from the incomplete combustion of coal, fossil fuel, and biomass, while OC is derived from both primary sources and secondary organic aerosols generated by photochemical reactions in the atmosphere (Yang et al., 2020). As shown in Fig. 2 (e-f) and Table S1, during the sampling period, the EC and OC were 2.2 ± 1.6 and 6.2 ± 3.3 μg/m^3, respectively, with an OC/EC ratio of 3.1 ± 0.8, lower than in summer (4.1) (Ding et al., 2021), and the higher ratio indicated the presence of prominent secondary organic aerosols (SOA) in ambient air (Zhang et al., 2017). The OC and EC in this study were 50% less than urban areas in YRD region and another background site of the YRD area (Lin'an city) (Feng et al., 2015).

The concentrations of SOC was calculated as following equation:

$$SOC = OC - EC*(OC/EC)\ min \quad (1)$$

where (OC/EC) min was the minimum OC/EC ratio during the study period (Lin et al., 2009). The WSOC and SOC were 4.0 ± 2.9 and 2.8 ± 1.5 μg/m^3, respectively. Fig. 3 compared the ratios of WSOC/OC and SOC/OC in this study with summer samples in the same site (Ding et al., 2021). It was clearly found that in winter time, the WSOC/OC was higher than that in summer, while the ratio of SOC/OC showed the opposite result. The atmospheric photochemical oxidation capacity in winter was relatively weaker than that in summer, resulting in less SOC formation. On the other hand, the new particles were mainly formed by aqueous phase reaction under high humidity conditions, thus the OC were usually water soluble (Fu et al., 2009; Ni et al., 2021). SO_4^{2-} and NO_3^- are two important inorganic anions of aerosols. During the whole campaign, the concentration of NO_3^- was 12.8 μg/m^3, about twice of SO_4^{2-} (6.1 μg/m^3), indicating NO_3^- was the dominant secondary inorganic component, resulting from the fact of increasing NOx and decreasing SO_2 pollution in atmospheric aerosols in China in recent years (Wang et al., 2016, 2019, 2020; Ge et al., 2019).

Table 1
Diurnal concentrations of dicarboxylic acids, ketocarboxylic acids, α-dicarbonyls in $PM_{2.5}$ in Chongming Island during the wintertime.

Compounds	Day(n = 29)	Night(n = 30)	Total(n = 59)
	Ave.±Std.(Min-Max)	Ave.±Std.(Min-Max)	Ave.±Std.(Min-Max)
Dicarboxylic acids (ng/m3)			
Oxalic,C2	189 ± 138 (47–682)	209 ± 163 (34–752)	199 ± 151 (34–752)
Malonic,C3	23 ± 12 (6.1–45)	18 ± 11 (3.9–46)	20 ± 12 (3.9–46)
Succinic,C4	23 ± 23 (1.8–106)	25 ± 23 (1.6–100)	24 ± 23 (1.6–106)
Glutaric,C5	9.8 ± 8.4 (3.2–45)	7.2 ± 5.5 (2.6–27)	8.5 ± 7.2 (2.6–45)
Adipic,C6	7.8 ± 4.5 (0.6–19)	7.8 ± 5.3 (1.1–22)	7.8 ± 4.9 (0.6–22)
Pimelic,C7	6.3 ± 2.9 (1.7–15)	5.6 ± 3.2 (2.7–14)	5.9 ± 3.1 (1.7–15)
Suberic,C8	1.2 ± 0.8 (0.2–3.8)	1.1 ± 0.8 (0.3–3.7)	1.1 ± 0.8 (0.2–3.8)
Azwlaic,C9	6.4 ± 3.4 (2.0–17)	6.4 ± 4.7 (2.2–22)	6.4 ± 4.1 (2.0–22)
Sebacic,C10	1.8 ± 0.9 (0.6–4.5)	1.8 ± 1.3 (0.6–5.9)	1.8 ± 1.1 (0.6–5.9)
Undecanedioic, C11	6.1 ± 12.8 (2.6–17)	4.7 ± 2.9 (2.6–13)	5.4 ± 2.9 (2.6–17)
Methylmalonic, iC4	15 ± 9.0 (2.6–42)	13 ± 5.3 (2.1–28)	14 ± 7.6 (2.1–42)
Methylsuccinic, iC5	11 ± 5.2 (2.1–22)	7.9 ± 4.0 (2.3–17)	9.2 ± 4.8 (2.1–22)
Methylglutaric, iC6	7.0 ± 5.2 (1.3–21)	6.9 ± 6.2 (1.3–27)	6.9 ± 5.7 (1.3–27)
Maleic,M	4.1 ± 2.0 (1.4–10)	3.7 ± 2.8 (1.7–16)	3.9 ± 2.3 (1.4–16)
Fumaric,F	5.2 ± 1.8 (2.0–9.7)	3.7 ± 1.6 (2.3–7.4)	4.4 ± 1.8 (2.0–9.7)
Methylmaleic,mM	7.0 ± 3.3 (2.0–17)	5.0 ± 2.3 (2.4–12)	6.0 ± 3.0 (2.0–17)
Phthalic,Ph	27 ± 19 (8.2–79)	19 ± 12 (4.5–52)	23 ± 16 (4.5–79)
Isophthalic,iPh	6.3 ± 3.2 (2.6–14)	4.9 ± 2.9 (1.6–12)	5.6 ± 3.1 (1.6–14)
Terephthalic,tPh	4.7 ± 2.2 (1.6–11)	3.8 ± 1.8 (1.6–9.0)	4.2 ± 2.1(1.6–11)
Ketopimelic,kC7	4.3 ± 1.5 (1.8–8.6)	2.9 ± 1.2 (2.0–6.8)	3.6 ± 1.5 (1.8–8.6)
Subtotal	364 ± 224 (94–1105)	355 ± 241 (105–1131)	360 ± 233 (94–1131)
Ketocarboxylic acids (ng/m3)			
Pyruvic,Pyr	15 ± 9.6 (0.9–44)	12 ± 4.7 (5.1–25)	13 ± 7.7 (0.9–44)
Glyoxylic,ωC2	31 ± 26 (5.9–132)	26 ± 21 (2.3–92)	29 ± 24 (2.3–132)
Subtotal	46 ± 32 (6.8–154)	37 ± 25 (13–111)	42 ± 29(6.8–154)
α-Dicarbonyls (ng/m3)			
Glyoxal,Gly	4.9 ± 3.7 (0.6–15)	4.5 ± 3.4 (1.6–16)	4.7 ± 3.5 (0.6–16)
Methyglyoxal, mGly	31 ± 21 (0.9–88)	22 ± 8.7 (1.9–44)	26 ± 16 (0.9–88)
Subtotal	36 ± 23 (1.5–99)	26 ± 11 (3.8–60)	31 ± 18 (1.5–99)
Total detected	446 ± 269 (107–1305)	419 ± 270 (135–1282)	433 ± 270 (107–1305)

3.2. Molecular characteristics and diurnal variations

The molecular characteristics of dicarboxylic acids, ketocarboxylic acids, and α-dicarbonyls during this study were summarized in Table 1, and the diurnal variations were provided in Fig. 4.

As shown in Table 1, the dicarboxylic acids concentration were 360 ± 233 ng/m^3, among which oxalic acid (C_2) was the most abundant individual, followed by phthalic acid (Ph), succinic acid (C_4), and malonic acid (C_3). This result was different from the result observed in summertime, during which C_2 was the most abundant target, followed by C_4 and C_3 (Ding et al., 2021). Ph is secondary product formed by photochemical oxidation reaction from aromatic hydrocarbons (e.g.

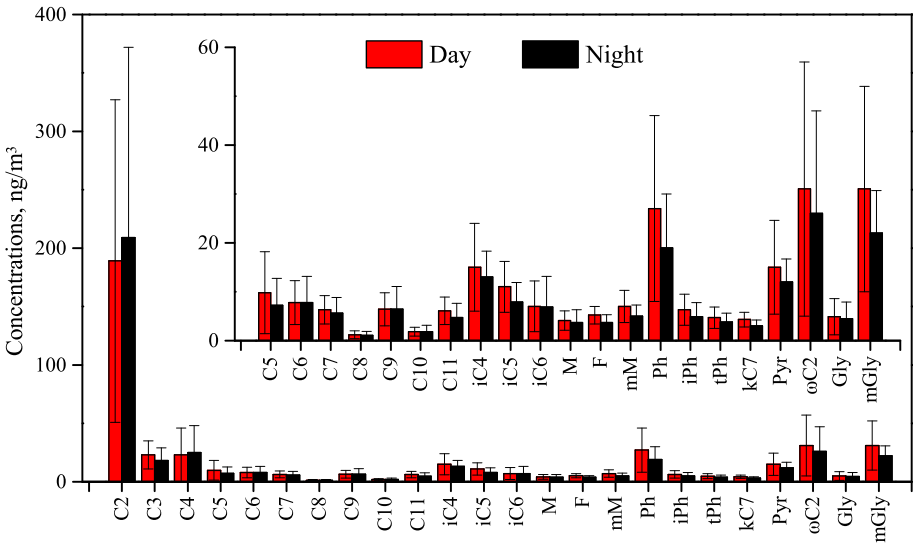

Fig. 4. Molecular distributions of dicarboxylic acids, ketocarboxylic acids, and α-dicarbonyls in the $PM_{2.5}$ samples collected at Chongming Island I winter.

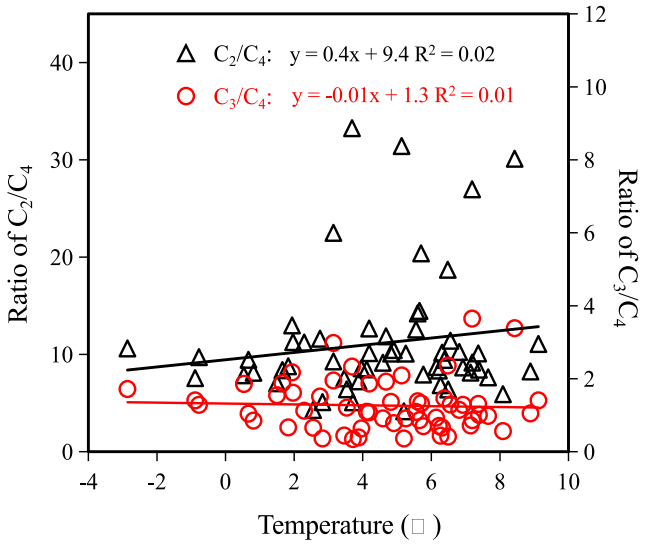

Fig. 5. Linear fit regression for temperature with C_2/C_4 and C_3/C_4 ratios during the wintertime sampling period.

PAHs) emitted from solid fuels burning (Jung et al., 2010). Therefore, the difference of molecular distribution might result from solid fuels combustion during heating period (detailed discussion in chapter 3.3.1). The concentration of oxalic acid was 199 ± 151 (ranging from 34 to 752) ng/m^3, accounting for 52% of the dicarboxylic acids. The concentration of oxalic acid in this study was significantly lower than those in Northern cities with coal heating in winter such as Xi'an (1379 ± 970 ng/m^3) (Wu et al., 2020) and Liaocheng (817 ± 544 ng/m^3) (Meng et al., 2020) and 6% lower than that observed in the summertime (Ding et al., 2021). The concentration of oxalic acid was 163 ng/m^3 at nighttime, 11% higher than that at the daytime (189 ± 138 ng/m^3, $p < 0.05$), different from that in summertime when no diurnal difference was found (Ding et al., 2021). The ratios of C_6/C_9 (Adipic/Azwlaic) and Ph/C_9 is often used to characterize the relative contribution of biogenic source and anthropogenic source (Jung et al., 2010; Meng et al., 2013). Table S2 provided the ratios of C_6/C_9 and Ph/C_9 in this study and other Asian cities in wintertime. Both C_6/C_9 and Ph/C_9 in Chongming Island were significantly higher than that in other cities, suggesting

Table 2
Meteorological conditions, concentrations and ratios of diacids in the four typical pollution events.

Items	Event 1 (N = 6)	Event 2 (N = 8)	Event 3 (N = 10)	Event 4 (N = 8)
Date	1.1–1.3	1.12–1.15	1.16–1.20	1.21–1.24
Relative humidity (%)	65 ± 9	81 ± 9	66 ± 10	69 ± 13
Temperature (°C)	4.5 ± 2.1	5.0 ± 1.8	4.6 ± 2.4	5.8 ± 1.8
1. Concentrations				
PM2.5 μg/m^3	63 ± 26	89 ± 38	85 ± 40	95 ± 31
K^+ μg/m^3	0.48 ± 0.2	0.51 ± 0.2	0.59 ± 0.2	0.79 ± 0.3
WSOC μg/m^3	4.6 ± 1.6	5.6 ± 2.0	4.8 ± 2.3	8.1 ± 3.4
levoglucosan, ng/m^3	48 ± 12	41 ± 9.0	64 ± 36	89 ± 32
C2, ng/m^3	224 ± 98	299 ± 187	242 ± 131	355 ± 163
Ph, ng/m^3	39 ± 19	41 ± 23	20 ± 8	29 ± 7
Total dicarboxylic acids, ng/m^3	413 ± 150	522 ± 284	431 ± 209	601 ± 221
Total ketocarboxylic acids, ng/m^3	41 ± 15	62 ± 39	58 ± 28	65 ± 25
Total α-Dicarbonyls, ng/m^3	28 ± 16	39 ± 13	37 ± 18	46 ± 18
Total detected diacids, TDCs, ng/m^3	482 ± 173	623 ± 323	525 ± 250	712 ± 245
2. Ratios				
C2/C4	8.8 ± 0.7	6.9 ± 2.3	9.4 ± 1.0	8.7 ± 1.3
C3/C4	1.1 ± 0.4	0.6 ± 0.3	1.2 ± 0.4	0.9 ± 0.4
C2/TDCs	0.45 ± 0.07	0.44 ± 0.07	0.45 ± 0.07	0.49 ± 0.09
C6/C9	1.4 ± 0.7	1.2 ± 0.3	0.8 ± 0.2	0.9 ± 0.2
Ph/C9	5.8 ± 2.0	6.0 ± 1.9	2.7 ± 0.7	2.5 ± 0.8
(lev/OC)%	0.71 ± 0.16	0.63 ± 0.14	0.79 ± 0.28	0.82 ± 0.24

anthropogenic sources dominated in the study site. Fig. 5 showed the relationship between ambient temperature and ratios of C_2/C_4 and C_3/C_4, the weak linear correlations indicated the ambient aerosols were mainly derived from the long-range transport of anthropogenic emission instead of the local sources (Ding et al., 2021; Meng et al., 2018).

The concentration of total ketocarboxylic acids was 42 ± 29 ng/m^3, of which glyoxylic acid (ωC_2) (29 ± 24 ng/m^3) was the most dominant species, following by pyruvic (Pyr). The total α-dicarbonyls concentration was 31 ± 18 ng/m^3 with a significantly larger contribution of methyglyoxal (mGly) than glyoxal (Gly) (26 ± 16 vs 4.7 ± 3.5 ng/m^3). Apart from the wider sources of mGly (Meng et al., 2013), the faster gas phase oxidation of Gly by OH radical could be the reasons for the higher

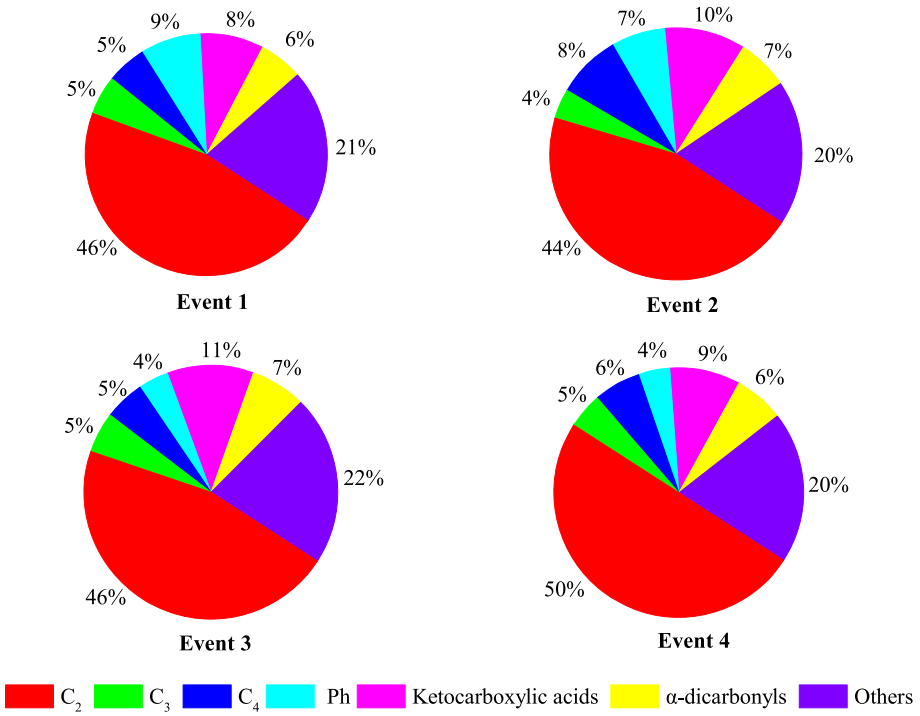

Fig. 6. Molecular compositions of dicarboxylic acids in the four events (TDCs means the total detected dicarboxylic acids and others means the other dicarboxylic acids of TDCs).

contribution of mGly (Cheng et al., 2013).

3.3. Typical pollution events

To further analyze the sources of $PM_{2.5}$ pollution during the polluted days, four periods with continuous high $PM_{2.5}$ concentrations were defined as pollution events (defined as Event 1, Event 2, Event 3, and Event 4, shown as gray shadow in Fig. 2). The following discussion will focus on the pollution characteristics of the four pollution events.

3.3.1. Molecular differences of diacids

As shown in Table 2, Event 4 had the highest concentration of $PM_{2.5}$ as well as C_2, total diacids, and total ketocarboxylic acids. Interestingly, although total dicarboxylic acids in Event 1 was the lowest, the Ph concentration during Event 1 (39 ng/m^3) was higher than that of Event 3 and Event 4 and slightly comparable to that of Event 2 (41 ng/m^3). As shown in Fig. 6, the relative contribution of Ph to the dicarboxylic acids in Event 1 was the highest (9%), following by Event 2 (7%), and Event 3 (4%) and Event 4 (4%). As shown in Table 2, C_6/C_9 and Ph/C_9 were

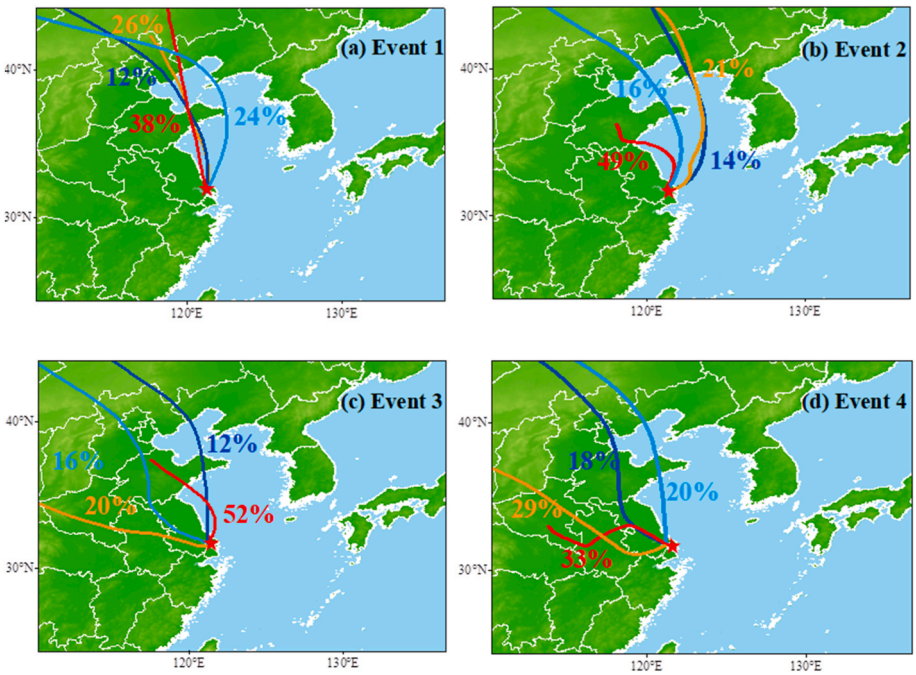

Fig. 7. Cluster analysis on the 48-h backward air mass trajectories of the samples collected during the four events.

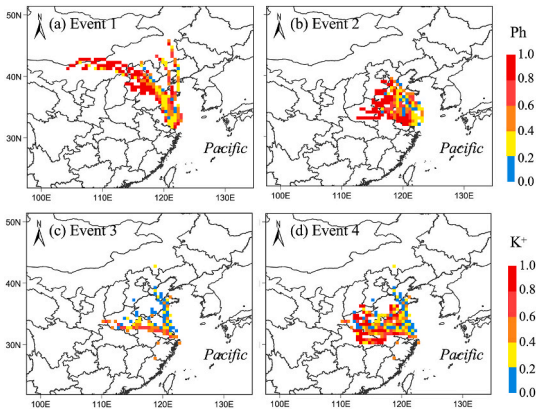

Fig. 8. The PSCF value of Ph in Event 1 (a) and Event 2 (b) and K^+ in Event 3 (c) and Event 4 (d).

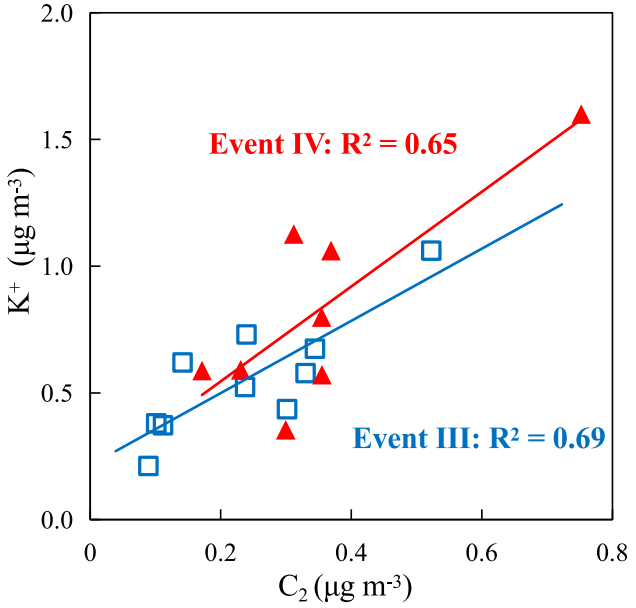

Fig. 9. The correlation between oxalic acid and K^+ during Event III and Event IV periods.

close in Event 1 and Event 2, indicating the potentially similar source of SOA in Event 1 and Event 2. Event 3 and Event 4 also had close ratios and similar sources. However, the ratios (especially for Ph/C_9) in Event 1 and Event 2 were significantly higher than that in the two latter events, indicating that Event 1 and Event 2 were affected more by anthropogenic source than that in Event 3 and Event 4.

As shown in Fig. 6, the highest proportion of oxalic acid in the total TDCs (Total detected diacids) was observed in Event 4, while lowest in Event 2. Previous studies confirmed that the ratio of C_2/C_4, C_3/C_4, and C_2/TDCs could be used to characterize the aging degree of atmospheric aerosols, and a lower ratio represented a fresher aerosol (Ho et al., 2015; Kunwar et al., 2017; Wang et al., 2012). The ratios in Event 1, Event 3, and Event 4 were close, higher than that in Event 2, indicating the aerosols in Event 2 was less aged. WSOC in aerosols comes from either primary source emissions or secondary photochemical oxidation, while C_2 and SO_4^{2-} are generally regarded as secondary products. Fig. S1 showed the correlation between WSOC and C_2 and SO_4^{2-} in the four events. In Event 2, the relationships were weak ($R^2 < 0.3$), compared to that in other events ($R^2 > 0.6$), again indicating that WSOC in Event 2 was relatively fresher.

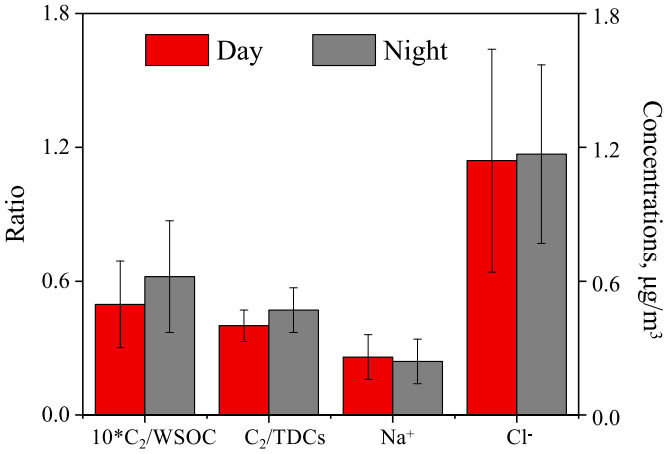

Fig. 10. Comparison of C_2/WSOC and C_2/TDCs ratios, and Na^+ and Cl^- concentrations in diurnal samples during the heavy pollution period in winter.

3.3.2. *The potential sources of the polluted events*

To further analyze the potential sources of the four typical pollution events, cluster analysis on the backward trajectory was carried out and the results were shown in Fig. 7. From Event 1 to Event 4, the air masses shifted from north to the southwest in space. During Event 1 and Event 2, the air masses originated from the northern China (e.g. Inner Mongolia and Shandong) where space heating was needed. As mentioned above, Event 1 and Event 2 had similar anthropogenic sources since the higher Ph was usually associated with coal combustion. The PSCF values of Ph in Fig. 8 also showed the higher values of Ph were consistently concentrated in the northern provinces in Event 1 and Event 2. Therefore, air masses discharged from coal combustion in these provinces transported to the sampling site was the main source of the target pollutants during Event 1 and Event 2. According to Fig. 7 (a-b), the air masses during Event 1 were transmitted over a long-range distance, while relatively short in Event 2. The shorter transport distance resulted in the fresher aerosols in Event 2, as mentioned above.

Levoglucosan (lev) and K^+ are generally considered as tracers for biomass burning (Jordan et al., 2006; Wang et al., 2014). As shown in Table 2, the concentrations of lev and K^+ and the ratio of lev/OC in Event 3 and Event 4 were significantly higher than that in Event 1 and Event 2, indicating that the SOA in Event 3 and Event 4 was most likely from biomass combustion. Furthermore, C_2 showed strong linear correlation with K^+ in Event 3 and Event 4 (Fig. 9), also indicating diacids in these two events were mostly originated from biomass burning. The fire point data (Fig. S2) and PSCF value of K^+ in Event 3 and Event 4 showed that the biomass burning emissions were mainly distributed in southern central Anhui province, southern Henan province and northern Hubei province. As shown in Figs. 7 (c), 20% of the air masses in Event 3 came from the provinces with frequent biomass burning, which had experienced a secondary aging process before reaching the sampling site through a long-distance transport. The aerosols derived from the provinces with frequent biomass burning might be the most important source of SOA in Event 3. Although 52% of the inland air masses from Shandong province in Event 3, the relative abundance and mass concentration of Ph were the lowest compared with other periods (Fig. 6 and Table 2), suggesting coal combustion was not the essential source in Event 3. In Event 4, the proportion of the air masses from the provinces with frequent biomass burning sharply increased to 62% (Fig. 7 (d)), along with denser fire points (Fig. S2 (b)), resulting in much higher K^+ and lev, again indicating a dominant source of biomass combustion.

3.3.3. *Formation mechanism of dicarboxylic acids and related SOA*

As described in section 3.2, the oxalic acid at night in winter was 11% higher than that in daytime, which was also significantly higher than that in summer (Ding et al., 2021). To further determine the reason

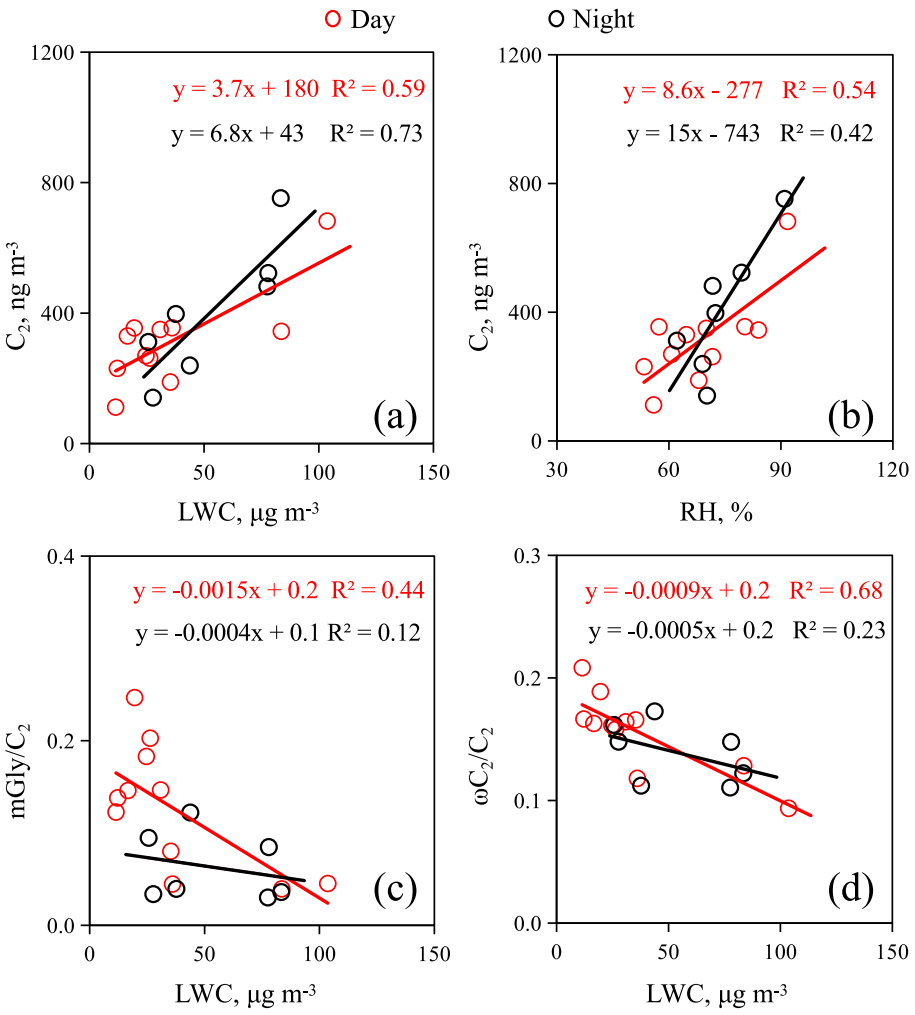

Fig. 11. Linear fit regressions for (a) LWC with C_2, (b) RH with C_2, (c) LWC with mGly/C_2, (d) LWC with $\omega C_2/C_2$ in the diurnal heavy haze samples.

for diurnal difference, samples from the heavily polluted period ($PM_{2.5}$ >75 μg/m^3) and the non-heavily polluted period ($PM_{2.5}$ <75 μg/m^3) were compared. As shown in Table S3, the concentration of C_2 during the heavy pollution period was more than three times that of the non-heavy pollution period, and the diurnal difference of oxalic acid was more obvious in the heavy pollution period (20% vs 8%). The decrease of the boundary layer height and the increase of precursor emission and/or the stronger oxidation formation process of C_2 at night during the polluted days might be the main reason (Meng et al., 2021).

Fig. 10 compared the ratios of oxalic acid to WSOC and C_2 to TDCs during the polluted days, it could be found that the ratios at night were significantly higher than that in the daytime, due to the decrease of the boundary layer height at night (Cheng et al., 2015). Besides, Na^+ and Cl^-, as two typical primary emission tracers (Meng et al., 2021), showed little diurnal difference during this period, indicating the effect of the precursor emissions was minor, thus C_2 formed by secondary oxidation might at night be the main reason for the diurnal difference. SO_4^{2-} is formed by the oxidation of SO_2 in the aqueous phase (Zhang et al., 2015b). A strong correlation between C_2 and SO_4^{2-} usually indicated a similar aqueous phase oxidation pathway (Meng et al., 2014; Warneck, 2003). In this study, the ratio of C_2/SO_4^{2-} (0.042 ± 0.022) at night during heavy pollution days was higher than that during the daytime (0.035 ± 0.014), again demonstrating the secondary formation of C_2 at night dominated in the diurnal difference. High concentration of O_3 and NO_2 at night could oxidize organic matter under high humidity condition at night (Wu et al., 2020). Previous studies confirmed C_2 was mainly formed by aqueous phase oxidation of precursors such as Gly, mGly, and ketocarboxylic acids (Carlton et al., 2006; Tong et al., 2016; Rapf et al., 2017), and some research also found that wintertime SOC formed by aqueous-phase transformation under high relative humidity condition could be an important contributor to carbonaceous aerosol, especially during haze periods in northern China (Zhang et al., 2015a). Therefore, the secondary formation of C_2 at night was mainly related to the aqueous phase oxidation process.

As shown in Fig. 11 (a-b), there was a strong correlation between ALWC and C_2 in the daytime (R^2 = 0.59), and a stronger correlation (R^2 = 0.73) at nighttime. There was also a good correlation between RH and C_2 (R^2 > 0.4). High ALWC and RH promoted the gas to aqueous phase conversion of mGly and ωC_2 precursors and subsequently the secondary oxidation of C_2 in the aerosol liquid phase (Fig. 11(c-d)). ALWC (78 μg/m^3) and RH (78% ± 9%) at night were higher than those in the daytime (ALWC: 36 μg/m^3; RH: 66% ± 10%), providing moist conditions at night, and further enhanced the formation of C_2 by promoting the distribution of Gly and mGly from gas phase to aqueous phase (Deshmukh et al., 2017).

3.3.4. *Size distributions of major diacids in haze periods*

Size-segregated samples were collected during Event 2 and Event 4. Strong correlations between the target diacids both in the two events were observed (Table S4). The size distribution characteristics of C_2, C_3, C_4, C_6, C_9, Ph, mGly, ωC_2 and TDCs were explored in Fig. 12. During Event 2, apart from C_6, the other dicarboxylic acid compounds showed obvious mono-modal distribution with a peak at 1.1–2.1 μm, indicating these dicarboxylic acids may experience a similar aerosol oxidation

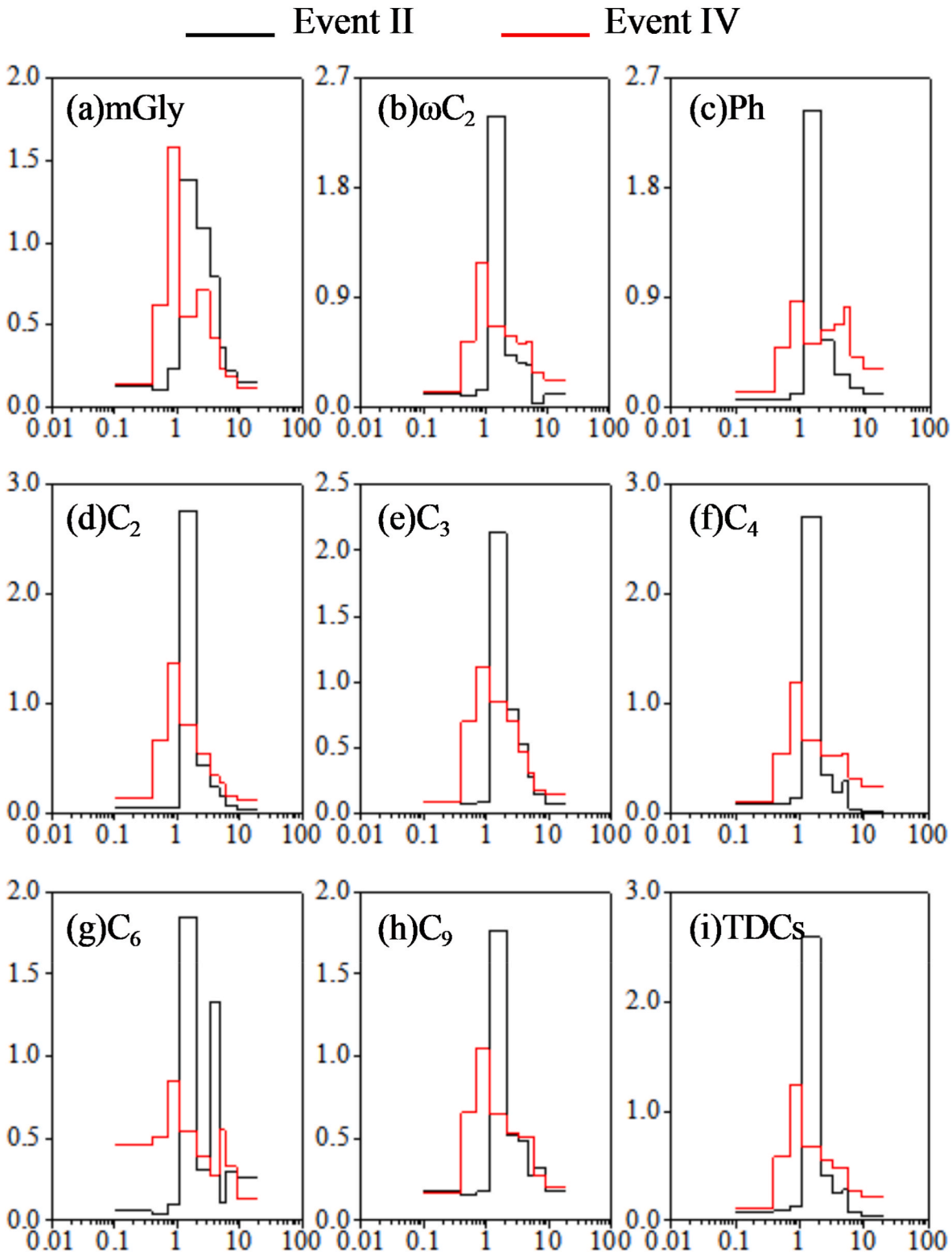

Fig. 12. Size distributions of dicarboxylic acids and related SOA during the different pollution events in winter.

process during the formation process. During Event 4, the dicarboxylic acids were concentrated in 0.7–1.1 μm, relatively finer than that in Event 2. The size distribution in this study was much different from that in summer, when dicarboxylic acids such as C_2 showed a bimodal size distribution pattern (Ding et al., 2021). The main reason is during summertime, the ambient temperature was much higher, the precursors in the fine modes could volatilize into the atmosphere and subsequently partition into the coarse mode aerosols (Wang et al., 2012). The fact that organic pollutants had a bimodal size distribution pattern during summer was also found for particulate amines, which again demonstrated a volatilization and redistribution on coarse model of organic pollutants (Du et al., 2021).

4. Summary and conclusion

The diurnal $PM_{2.5}$ samples were collected in Chongming Island and EC, OC, WSOC, IC, dicarboxylic acids, ketocarboxylic acids, α-dicarbonyls, and levoglucosan were detected. During the sampling period, the total concentration of dicarboxylic acids was 360 ± 233 ng/m^3, of which C_2, as the dominant specie, was 199 ± 151 ng/m^3. Oxalic acid was significantly different from other substances in diurnal distribution, with higher concentration at night, indicating more C_2 was produced by the aqueous phase reaction at night. Four typical pollution events were observed during the field campaign. Event 1 and Event 2 were mainly caused by the air mass transport of coal emission from northern provinces with space heating. Events 3 and 4 were chiefly caused by long distance transport of air masses from biomass burning. During the haze days, the dicarboxylic acids and related SOA were mainly formed through aqueous phase reaction, which was enhanced at night. The dicarboxylic acids followed a mono-modal distribution in winter, obviously different from that in summer, mainly due to the weak volatilization in winter with low ambient temperature.

CRediT authorship contribution statement

Wei Du: Conceptualization, Formal analysis, Writing – original draft, Writing – review & editing. **Zhijian Ding:** Conceptualization, Formal analysis, Writing – original draft, Writing – review & editing. **Yali Lei:** Writing – review & editing. **Si Zhang:** Writing – review & editing. **Can Wu:** Writing – review & editing. **Fan Zhang:** Writing – review & editing. **Fanglin Wang:** Writing – review & editing. **Shaojun Lv:** Writing – review & editing. **Xiaodi Liu:** Writing – review & editing. **Jingjing Meng:** Writing – review & editing. **Gehui Wang:** Funding acquisition, Writing – review & editing.

Declaration of competing interest

The authors declare that they have no known competing financial interests or personal relationships that could have appeared to influence the work reported in this paper.

Data availability

Data will be made available on request.

Acknowledgments

This work was financially supported by the National Natural Science Foundation of China (No. 41773117), Development Projects of Shanghai Science and Technology Commission (No.20dz1204000), ECNU Happiness Flower Program and the Fundamental Research Funds for the Central Universities and Key Research.

Appendix A. Supplementary data

Supplementary data to this article can be found online at https://doi.org/10.1016/j.atmosenv.2022.119320.

References

Bilde, M., Barsanti, K., Booth, M., Cappa, C.D., Donahue, N.M., Emanuelsson, E.U., McFiggans, G., Krieger, U.K., Marcolli, C., Tropping, D., Ziemann, P., Barley, M., Clegg, S., Dennis-Smither, B., Hallquist, M., Hallquist, A.M., Khlystov, A., Kulmala, M., Mogensen, D., Percival, C.J., Pope, F., Reid, J.P., da Silva, M., Rosenoern, T., Salo, K., Soonsin, V.P., Yli-Juuti, T., Prisle, N.L., Pagels, J., Rarey, J., Zardini, A.A., Riipinen, I., 2015. Saturation vapor pressures and transition enthalpies of low-volatility organic molecules of atmospheric relevance: from dicarboxylic acids to complex mixtures. Chem. Rev. 115, 4115–4156. https://doi.org/10.1021/cr5005502.

Cai, C.Y., Li, J.Y., Di, W., Wang, X.L., Tsang, D.C.W., Li, X.D., Sun, J.T., Zhu, L.H., Shen, H.Z., Tao, S., Liu, W.X., 2017. Spatial distribution, emission source and health risk of parent PAHs and derivatives in surface soils from the Yangtze River Delta, eastern China. Chemosphere 178, 301–308. https://doi.org/10.1016/j.chemosphere.2017.03.057.

Carlton, A.G., Turpin, B.J., Lim, H.J., Altieri, K.E., Seitzinger, S., 2006. Link between isoprene and secondary organic aerosol (SOA): pyruvic acid oxidation yields low volatility organic acids in clouds. Geophys. Res. Lett. 33 https://doi.org/10.1029/2005gl025374.

Cheng, C.L., Wang, G.H., Zhou, B.H., Meng, J.J., Li, J.J., Cao, J.J., Xiao, S., 2013. Comparison of dicarboxylic acids and related compounds in aerosol samples collected in Xi'an, China during haze and clean periods. Atmos. Environ. 81, 443–449. https://doi.org/10.1016/j.atmosenv.2013.09.013.

Cheng, C., Wang, G.H., Meng, J.J., Wang, Q.Y., Cao, J.J., Li, J.J., et al., 2015. Size-resolved airborne particulate oxalic and related secondary organic aerosol species in the urban atmosphere of Chengdu, China. Atmos. Res. 161, 134–142.

Chow, J.C., Watson, J.G., Chen, L.W.A., Arnott, W.P., Moosmuller, H., Fung, K., 2004. Equivalence of elemental carbon by thermal/optical reflectance and transmittance with different temperature protocols. Environ. Sci. Technol. 38, 4414–4422. https://doi.org/10.1021/es034936u.

Deshmukh, D.K., Kawamura, K., Deb, M.K., Boreddy, S.K.R., 2017. Sources and formation processes of water-soluble dicarboxylic acids, -oxocarboxylic acids, -dicarbonyls, and major ions in summer aerosols from eastern central India. J. Geophys. Res. Atmos. 122, 3630–3652.

Ding, Z., Du, W., Wu, C., Cheng, C., Meng, J., Li, D., et al., 2021. Summertime atmospheric dicarboxylic acids and related SOA in the background region of Yangtze River Delta, China: implications for heterogeneous reaction of oxalic acid with sea salts. Sci. Total Environ. 757, 143741-143741.

Du, W., Wang, X.P., Yang, F.Q., Bai, K.X., Wu, C., Liu, S.J., Wang, F.L., Lv, S.J., Chen, Y. B., Wang, J.Z., Liu, W.L., Wang, L.J., Chen, X.L., Wang, G.H., 2021. Particulate amines in the background atmosphere of the Yangtze River Delta, China: concentration, size distribution, and sources. Adv. Atmos. Sci. https://doi.org/10.1007/s00376-021-0274-0.

Ervens, B., Turpin, B.J., Weber, R.J., 2011. Secondary organic aerosol formation in cloud droplets and aqueous particles (aqSOA): a review of laboratory, field and model studies. Atmos. Chem. Phys. 11, 11069–11102. https://doi.org/10.5194/acp-11-11069-2011.

Feng, J.L., Hu, J.C., Xu, B.H., Hu, X.L., Sun, P., Han, W.L., Gu, Z.P., Yu, X.M., Wu, M.H., 2015. Characteristics and seasonal variation of organic matter in PM2.5 at a regional background site of the Yangtze River Delta region, China. Atmos. Environ. 123, 288–297. https://doi.org/10.1016/j.atmosenv.2015.08.019.

Fu, P.Q., Kawamura, K., Chen, J., Barrie, L.A., 2009. Isoprene, monoterpene, and sesquiterpene oxidation products in the high arctic aerosols during late winter to early summer. Environ. Sci. Technol. 43, 4022–4028.

Ge, S.S., Wang, G.H., Zhang, S., Li, D.P., Xie, Y.N., Wu, C., Yuan, Q., Chen, J.M., Zhang, H.L., 2019. Abundant NH3 in China enhances atmospheric HONO production by promoting the heterogeneous reaction of SO2 with NO2. Environ. Sci. Technol. 53, 14339–14347. https://doi.org/10.1021/acs.est.9b04196.

Haque, M.M., Fang, C., Schnelle-Kreis, J., Abbaszade, G., Liu, X.Y., Bao, M.Y., Zhang, W. Q., Zhang, Y.L., 2020. Regional haze formation enhanced the atmospheric pollution levels in the Yangtze River Delta region, China: implications for anthropogenic sources and secondary aerosol formation. Sci. Total Environ. 728 https://doi.org/10.1016/j.scitotenv.2020.138013.

Ho, K.F., Huang, R.J., Kawamura, K., Tachibana, E., Lee, S.C., Ho, S.S.H., Zhu, T., Tian, L., 2015. Dicarboxylic acids, ketocarboxylic acids, alpha-dicarbonyls, fatty acids and benzoic acid in PM2.5 aerosol collected during CAREBeijing-2007: an effect of traffic restriction on air quality. Atmos. Chem. Phys. 15, 3111–3123. https://doi.org/10.5194/acp-15-3111-2015.

Jordan, T.B., Seen, A.J., Jacobsen, G.E., 2006. Levoglucosan as an atmospheric tracer for woodsmoke. Atmos. Environ. 40, 5316–5321.

Jung, J., Tsatsral, B., Kim, Y.J., Kawamura, K., 2010. Organic and inorganic aerosol compositions in Ulaanbaatar, Mongolia, during the cold winter of 2007 to 2008: dicarboxylic acids, ketocarboxylic acids, and alpha-dicarbonyls. J. Geophys. Res. Atmos. 115 https://doi.org/10.1029/2010jd014339.

Kawamura, K., Okuzawa, K., Aggarwal, S.G., Irie, H., Kanaya, Y., Wang, Z., 2013a. Determination of gaseous and particulate carbonyls (glycolaldehyde, hydroxyacetone, glyoxal, methylglyoxal, nonanal and decanal) in the atmosphere at Mt. Tai. Atmos. Chem. Phys. 13, 5369–5380, 13,10(2013-05-28).

Kawamura, K., Tachibana, E., Okuzawa, K., Aggarwal, S.G., Kanaya, Y., Wang, Z.F., 2013b. High abundances of water-soluble dicarboxylic acids, ketocarboxylic acids and alpha-dicarbonyls in the mountaintop aerosols over the North China Plain during wheat burning season. Atmos. Chem. Phys. 13, 8285–8302. https://doi.org/10.5194/acp-13-8285-2013.

Kawamura, K., Bikkina, S., 2016. A review of dicarboxylic acids and related compounds in atmospheric aerosols: molecular distributions, sources and transformation. Atmos. Res. 170, 140–160. https://doi.org/10.1016/j.atmosres.2015.11.018.

Kunwar, B., Torii, K., Kawamuraa, K., 2017. Springtime influences of Asian outflow and photochemistry on the distributions of diacids, oxoacids and alpha-dicarbonyls in the aerosols from the western North Pacific Rim. Tellus Ser. B Chem. Phys. Meteorol. 69 https://doi.org/10.1080/16000889.2017.1369341.

Li, J.J., Wang, G.H., Zhou, B.H., Cheng, C.L., Cao, J.J., Shen, Z.X., An, Z.S., 2012. Airborne particulate organics at the summit (2060 m, a.s.l.) of Mt. Hua in central China during winter: implications for biofuel and coal combustion. Atmos. Res. 106, 108–119. https://doi.org/10.1016/j.atmosres.2011.11.012.

Lin, P., Hu, M., Deng, Z., Slanina, J., Han, S., Kondo, Y., et al., 2009. Seasonal and diurnal variations of organic carbon in PM2.5 in Beijing and the estimation of secondary organic carbon. J. Geophys. Res. Atmos. 114.

Liu, J., Zhou, S., Zhang, Z., Kawamura, K., Zhao, W., Wang, X., Shao, M., Jiang, F., Liu, J., Sun, X., Hang, J., Zhao, J., Pei, C., Zhang, J., Fu, P., 2021. Characterization of dicarboxylic acids, oxoacids, and α-dicarbonyls in PM2.5 within the urban boundary layer in southern China: sources and formation pathways. Environ. Pollut. 285, 117185.

Meng, J.J., Li, Z., Zhou, R.W., Chen, M., Li, Y.Y., Yi, Y.N., et al., 2021. Enhanced photochemical formation of secondary organic aerosols during the COVID-19 lockdown in Northern China. Sci. Total Environ. 758.

Meng, J., Wang, G., Li, J., Cheng, C., Ren, Y., Huang, Y., Cheng, Y., Cao, J., Zhang, T., 2014. Seasonal characteristics of oxalic acid and related SOA in the free troposphere of Mt. Hua, central China: implications for sources and formation mechanisms. Sci. Total Environ. 493, 1088–1097. https://doi.org/10.1016/j.scitotenv.2014.04.086.

Meng, J.J., Wang, G.H., Li, J.J., Cheng, C.L., Cao, J.J., 2013. Atmospheric oxalic acid and related secondary organic aerosols in Qinghai Lake, a continental background site in Tibet Plateau. Atmos. Environ. 79, 582–589. https://doi.org/10.1016/j.atmosenv.2013.07.024.

Meng, J.J., Wang, G.H., Hou, Z.F., Liu, X.D., Wei, B.J., Wu, C., Cao, C., Wang, J.Y., Li, J. J., Cao, J.J., Zhang, E.X., Dong, J., Liu, J.Z., Ge, S.S., Xie, Y.N., 2018. Molecular distribution and stable carbon isotopic compositions of dicarboxylic acids and related SOA from biogenic sources in the summertime atmosphere of Mt. Tai in the North China Plain. Atmos. Chem. Phys. 18, 15069–15086. https://doi.org/10.5194/acp-18-15069-2018.

Meng, J.J., Liu, X.D., Hou, Z.F., Yi, Y.N., Yan, L., Li, Z., Cao, J.J., Li, J.J., Wang, G.H., 2020. Molecular characteristics and stable carbon isotope compositions of dicarboxylic acids and related compounds in the urban atmosphere of the North China Plain: implications for aqueous phase formation of SOA during the haze periods. Sci. Total Environ. 705 https://doi.org/10.1016/j.scitotenv.2019.135256.

Meng, J.J., Li, Z., Zhou, R.W., Chen, M., Li, Y.Y., Yi, Y.N., Ding, Z.J., Li, H.J., Yan, L., Hou, Z.F., Wang, G.H., 2021. Enhanced photochemical formation of secondary organic aerosols during the COVID-19 lockdown in Northern China. Sci. Total Environ. 758.

Ni, X., Pan, Y.P., Shao, P., Tian, S.L., Zong, Z., Gu, M.N., et al., 2021. Size distribution and formation processes of aerosol water-soluble organic carbon during winter and summer in urban Beijing. Atmos. Environ. 244.

Petaja, T., Jarvi, L., Kerminen, V.M., Ding, A.J., Sun, J.N., Nie, W., Kujansuu, J., Virkkula, A., Yang, X.Q., Fu, C.B., Zilitinkevich, S., Kulmala, M., 2016. Enhanced air pollution via aerosol-boundary layer feedback in China. Sci. Rep. 6 https://doi.org/10.1038/srep18998.

Rapf, R.J., Dooley, M.R., Kappes, K., Perkins, R.J., Vaida, V., 2017. pH dependence of the aqueous photochemistry of alpha-keto acids. J. Phys. Chem. A 121, 8368–8379. https://doi.org/10.1021/acs.jpca.7b08192.

Rogge, W.F., Hildemann, L.M., Mazurek, M.A., Cass, G.R., Simoneit, B.R.T., 1991. Sources of fine organic aerosol. 1. Charbroilers and meat cooking operations. Environ. Sci. Technol. 25, 1112–1125.

Song, C.B., Wu, L., Xie, Y.C., He, J.J., Chen, X., Wang, T., Lin, Y.C., Jin, T.S., Wang, A.X., Liu, Y., Dai, Q.L., Liu, B.S., Wang, Y.N., Mao, H.J., 2017. Air pollution in China: status and spatiotemporal variations. Environ. Pollut. 227, 334–347. https://doi.org/10.1016/j.envpol.2017.04.075.

Tong, H.J., Kourtchev, I., Pant, P., Keyte, I.J., O'Connor, I.P., Wenger, J.C., Pope, F.D., Harrison, R.M., Kalberer, M., 2016. Molecular composition of organic aerosols at urban background and road tunnel sites using ultra-high resolution mass spectrometry. Faraday Discuss 189, 51–68. https://doi.org/10.1039/c5fd00206k.

Wang, G., Xie, M., Hu, S., Gao, S., Tachibana, E., Kawamura, K., 2010. Dicarboxylic acids, metals and isotopic compositions of C and N in atmospheric aerosols from inland China: implications for dust and coal burning emission and secondary aerosol formation. Atmos. Chem. Phys. 10, 6087–6096. https://doi.org/10.5194/acp-10-6087-2010.

Wang, G., Zhang, R., Gomez, M.E., Yang, L., Zamora, M.L., Hu, M., Lin, Y., Peng, J., Guo, S., Meng, J., Li, J., Cheng, C., Hu, T., Ren, Y., Wang, Y., Gao, J., Cao, J., An, Z., Zhou, W., Li, G., Wang, J., Tian, P., Marrero-Ortiz, W., Secrest, J., Du, Z., Zheng, J., Shang, D., Zeng, L., Shao, M., Wang, W., Huang, Y., Wang, Y., Zhu, Y., Li, Y., Hu, J., Pan, B., Cai, L., Cheng, Y., Ji, Y., Zhang, F., Rosenfeld, D., Liss, P.S., Duce, R.A., Kolb, C.E., Molina, M.J., 2016. Persistent sulfate formation from London Fog to Chinese haze. Proc. Natl. Acad. Sci. U. S. A 113, 13630–13635. https://doi.org/10.1073/pnas.1616540113.

Wang, G.H., Cheng, C.L., Li, J.J., Zhou, B.H., Xie, M.J., Hu, S.Y., Kawamura, K., Chen, Y., 2011. Molecular composition and size distribution of sugars, sugar-alcohols and carboxylic acids in airborne particles during a severe urban haze event caused by wheat straw burning. Atmos. Environ. 45, 2473–2479. https://doi.org/10.1016/j.atmosenv.2011.02.045.

Wang, G., Cheng, C.L., Huang, Y., Tao, J., Ren, Y.Q., Wu, F., et al., 2014. Evolution of aerosol chemistry in Xi'an, inland China, during the dust storm period of 2013-Part 1: sources, chemical forms and formation mechanisms of nitrate and sulfate. Atmos. Chem. Phys. 14, 11571–11585.

Wang, G.H., Kawamura, K., Cheng, C.L., Li, J.J., Cao, J.J., Zhang, R.J., Zhang, T., Liu, S. X., Zhao, Z.Z., 2012. Molecular distribution and stable carbon isotopic composition of dicarboxylic acids, ketocarboxylic acids, and alpha-dicarbonyls in size-resolved atmospheric particles from Xi'an city, China. Environ. Sci. Technol. 46, 4783–4791. https://doi.org/10.1021/es204322c.

Wang, J., Zhang, X.F., Ling, W.T., Liu, R., Liu, J., Kang, F.X., Gao, Y.Z., 2017. Contamination and health risk assessment of PAHs in soils and crops in industrial areas of the Yangtze River Delta region, China. Chemosphere 168, 976–987. https://doi.org/10.1016/j.chemosphere.2016.10.113.

Wang, W.F., Yu, J., Cui, Y., He, J., Xue, P., Cao, W., Ying, H.M., Gao, W.K., Yan, Y.C., Hu, B., Xin, J.Y., Wang, L.L., Liu, Z.R., Sun, Y., Ji, D.S., Wang, Y.S., 2018. Characteristics of fine particulate matter and its sources in an industrialized coastal city, Ningbo, Yangtze River Delta, China. Atmos. Res. 203, 105–117. https://doi.org/10.1016/j.atmosres.2017.11.033.

Wang, Y., Chen, Y., Wu, Z., Shang, D., Bian, Y., Du, Z., et al., 2020. Mutual promotion between aerosol particle liquid water and particulate nitrate enhancement leads to severe nitrate-dominated particulate matter pollution and low visibility. Atmos. Chem. Phys. 20, 2161–2175.

Wang, Y., Li, W., Gao, W., Liu, Z., Tian, S., Shen, R., et al., 2019. Trends in particulate matter and its chemical compositions in China from 2013-2017. Sci. China Earth Sci. 62, 1857–1871.

Warneck, P., 2003. In-cloud chemistry opens pathway to the formation of oxalic acid in the marine atmosphere. Atmos. Environ. 37, 2423–2427. https://doi.org/10.1016/s1352-2310(03)00136-5.

Wu, C., Zhang, S., Wang, G.H., Lv, S.J., Li, D.P., Liu, L., et al., 2020. Efficient heterogeneous formation of ammonium nitrate on the saline mineral particle surface in the atmosphere of east asia during dust storm periods. Environ. Sci. Technol. 54, 15622–15630.

Xu, J.S., Xu, H.H., Xiao, H., Tong, L., Snape, C.E., Wang, C.J., He, J., 2016. Aerosol composition and sources during high and low pollution periods in Ningbo, China. Atmos. Res. 178, 559–569. https://doi.org/10.1016/j.atmosres.2016.05.006.

Yang, J., Zhao, W.Y., Wei, L.F., Zhang, Q., Zhao, Y., Hu, W., Wu, L.B., Li, X.D., Pavuluri, C.M., Pan, X.L., Sun, Y.L., Wang, Z.F., Liu, C.Q., Kawamura, K., Fu, P.Q., 2020. Molecular and spatial distributions of dicarboxylic acids, oxocarboxylic acids, and alpha-dicarbonyls in marine aerosols from the South China Sea to the eastern Indian Ocean. Atmos. Chem. Phys. 20, 6641–6660. https://doi.org/10.5194/acp-20-6841-2020.

Yu, Q., Chen, J., Cheng, S.M., Qin, W.H., Zhang, Y.P., Sun, Y.W., Ahmad, M., 2021. Seasonal variation of dicarboxylic acids in PM2.5 in Beijing: implications for the formation and aging processes of secondary organic aerosols. Sci. Total Environ. 763 https://doi.org/10.1016/j.scitotenv.2020.142964.

Zhang, Q., Shen, Z.X., Cao, J.J., Zhang, R.J., Zhang, L.M., Huang, R.J., Zheng, C.J., Wang, L.Q., Liu, S.X., Xu, H.M., Zheng, C.L., Liu, P.P., 2015a. Variations in $PM_{2.5}$, TSP, BC, and trace gases (NO_2, SO_2, and O_3) between haze and non-haze episodes in winter over Xi'an, China. Atmos. Environ. 112, 64–71.

Zhang, Q., Ning, Z., Shen, Z.X., Li, G.L., Zhang, J.K., Lei, Y.L., Xu, H.M., Sun, J., Zhang, L. M., Dane, W., Nirmal, K.J., Gong, X.S., 2017. Variations of aerosol size distribution, chemical composition and optical properties from roadside to ambient environment: a case study in Hong Kong, China. Atmos. Environ. 166, 234–243.

Zhang, R.Y., Wang, G.H., Guo, S., Zarnora, M.L., Ying, Q., Lin, Y., Wang, W.G., Hu, M., Wang, Y., 2015b. formation of urban fine particulate matter. Chem. Rev. 115, 3803–3855. https://doi.org/10.1021/acs.chemrev.5b00067.

Zhang, Y.L., Kawamura, K., Cao, F., Lee, M., 2016. Stable carbon isotopic compositions of low-molecular-weight dicarboxylic acids, oxocarboxylic acids, -dicarbonyls, and fatty acids: implications for atmospheric processing of organic aerosols. J. Geophys. Res. Atmos. 121, 3707–3717. https://doi.org/10.1002/2015jd024081.